Kinetic modeling of rotational nonequilibrium in chemical lasers. A comparison of three models applied to the Cl_2/HI/He system

Yakir ReuvenAvinoam Ben-ShaulMichael Baer

Citation: **51**, (1980); doi: 10.1063/1.327406
View online: http://dx.doi.org/10.1063/1.327406
View Table of Contents: http://aip.scitation.org/toc/jap/51/1
Published by the American Institute of Physics

RIGHTSLINK
Copyright Clearance Center

Kinetic modeling of rotational nonequilibrium in chemical lasers. A comparison of three models applied to the Cl_2/HI/He system

Yakir Reuven[a)]
Department of Theoretical Physics and Applied Mathematics, Soreq Nuclear Research Centre, Yavne, Israel
Avinoam Ben-Shaul
Department of Physical Chemistry, The Hebrew University of Jerusalem, Jerusalem, Israel
Michael Baer
Department of Theoretical Physics and Applied Mathematics, Soreq Nuclear Research Centre, Yavne, Israel and Department of Chemical Physics, The Weizmann Institute, Rehovot, Israel

(Received 11 January 1979; accepted for publication 23 May 1979)

In this study three theoretical models which yield the temporal evolution of photon densities and population levels for a pulsed chemical laser are compared. The models are applied to the Cl_2/HI/He chemical laser system. The simplest one is the well-known Boltzmann equilibrium model (BEQM) which assumes instantaneous rotational equilibrium throughout the lasing period. This assumption is removed in the detailed rotational nonequilibrium model (DRNM) which follows the time development of each vib-rotational population level separately. A third model, recently introduced by Baer, Top, and Alfassi, is an approximate rotational relaxation model (ARRM) which represents the rotational distribution in each vibrational level as a linear combination of three known functions with time-dependent coefficients. The main conclusions are as follows: (1) The BEQM is inadequate for providing the properties of a laser operating under low and intermediate inert-gas pressures. It can serve at most to derive an upper bound for the actual laser performance. (2) The ARRM provides very good estimates of total laser energy and efficiency as well as of more detailed properties, such as band intensities and the temporal behavior of the vibrational populations, for a wide range of pressures. (3) The use of the DRNM cannot be avoided if fine details, such as spectral distribution of output energy or rotational energy profiles, are required.

PACS numbers: 42.55.Ks, 82.20.Mj, 82.20.Wt

I. INTRODUCTION

Indications of rotational nonequilibrium in low-pressure chemical lasers on the one hand,[1-8] and direct experimental determinations[9-13] of rotational relaxation rates on the other, have stimulated the inclusion of rotational nonequilibrium effects in kinetic modeling studies of molecular lasers.[3,14-24] Evidence for rotational nonequilibrium is provided by, for example, simultaneous multiline operation, and R-branch and pure rotational transitions. Chemiluminescence measurements,[11,25] double resonance,[9,10] and laser infrared fluorescence experiments[13] and theoretical models based on the exponential gap representation of rate constants[11,12,26] indicate that the rate of rotational relaxation decreases exponentially with the rotational quantum number J.

The rotational equilibrium assumption, which commonly was employed in the early modeling studies of chemical and other molecular lasers,[4,27] states that rotational relaxation is practically instantaneous on the time scale of all the other rate processes in the laser cavity, excluding translational relaxation but including, in particular, stimulated emission. This assumption is valid when a buffer gas which enhances (almost selectively) rotational relaxation is added to the lasing mixture; however, it is doubtful at intermediate pressures, especially for high J values, and is generally inadequate at low buffer gas pressures. The most important practical aspect in investigating the role of rotational relaxation in chemical lasers is the significant enhancement of the laser efficiency upon raising the rate of R-T transfer.[2,14,15,18]

The abandonment of the rotational equilibrium assumption in the kinetic description of (infrared) molecular lasers means that, instead of a few master equations governing the rate of change of the vibrational populations and the radiation densities of the few lasing transitions, one has to solve a large set of independent rate equations corresponding to the various vib-rotational levels and transitions. Moreover, instead of a few rotationally averaged rate constants, one needs detailed information about a multitude of vibrotational reactive and energy transfer rate constants. The latter problem is solved by the rapid accumulation of detailed rate constants. The more technical obstacle of solving a multitude of (coupled nonlinear) rate equations, even with the aid of fast integration procedures, is considerably more difficult. For systems involving a large number of significantly populated levels, such as chemical or electrical CO lasers or the H_2/F_2 laser system, the solution of all the detailed rate equations is an extremely complex problem.

An approximate model for rotational relaxation aimed at reducing the number of laser rate equations has recently been suggested.[21] The central assumption of this model is that the rotational distribution function within a given vibrational manifold can be expressed as a time-dependent super-

---

[a)] Part of a Ph.D. thesis to be submitted by Y. Reuven to the Department of Physical Chemistry, the Hebrew University of Jerusalem.

RIGHTSLINK

TABLE I. The kinetic scheme.

Initiation

$$Cl_2 \xrightarrow[\text{flash}]{h\nu} 2Cl \tag{R1}$$

Pumping

$$Cl + HI \rightarrow HCl(V,J) + I \tag{R2}$$

Reverse reaction

$$HCl(V=4,J) + I \rightarrow Cl + HI \tag{R3}$$

Radiation

$$HCl(V,J-1) \rightarrow HCl(V-1,J) + h\nu_{VJ} \tag{R4}$$

Relaxations

R-R,T

$$HCl(V,J) + M \rightarrow HCl(V,J \pm 1) + M \tag{R5}$$

V-T

$$HCl(V,J) + M_i \rightarrow HCl(V',J) + M_i\,, \quad V' < V \tag{R6}$$

where $M = \sum_i M_i$; $M_i = Cl_2, Cl, HI, I, HCl, He$

V-V

$$HCl(V,J) + HCl(V',J') \rightleftarrows HCl(V \pm 1,J) + HCl(V' \mp 1,J') \tag{R7}$$

position of three predetermined distributions, one of which is the Boltzmann equilibrium distribution. In this paper we test this model by comparing its predictions with a detailed solution of the vib-rotational rate equations of the Cl + HI →HCl + I chemical laser. This sytem involves many relevant levels and transitions but the solution of the rate equations governing its time evolution is still manageable. The detailed information about the kinetic behavior of this system, obtained by such treatment, is in itself of interest. To complete the analysis we compare both the approximate and detailed models with a simplified code based on the rotational equilibrium assumption.

II. THE KINETIC MODELS

The pumping reaction in the Cl_2/HI laser system is

$$Cl + HI \rightarrow HCl(V,J) + I, \tag{1}$$

where V,J denotes the vib-rotational level. The exothermicity of this reaction suffices to populate the first five ($V = 0$ – 4) vibrational levels of HCl. The number of energetically open rotational levels is 30, 28, 25, 19, and 9 for $V = 0,1,2,3,$ and 4, respectively.[28] All of these vib-rotational levels as well as all the possible P-branch transitions in the bands $V = 4 \rightarrow 3$, $3 \rightarrow 2$, $2 \rightarrow 1$, and $1 \rightarrow 0$ are included in the kinetic analysis. The Cl atoms are generated by flash photolysis of Cl_2 molecules. The kinetic scheme is summarized in Table I. Except for several modifications, the numerical values of the various rate constants are identical to those employed in Ref. 21. The initial mixture in the laser cavity contains Cl_2, HI, and He at various ratios and concentrations.

The three kinetic models compared in this paper differ in the way the vib-rotational level populations are treated. With regard to the treatment of the radiation densities (see below), the models are essentially identical. In all cases we assume that the rate processes and the level and photon populations are uniform in the volume of the laser cavity. Also, since except under the extreme condition of rotational nonequilibrium the gain of an R-branch transition is lower than that of a P-branch transition originating at the same V,J level,[2,27] only P-branch transitions are taken into account.

Consider first the most detailed model, the detailed rotational nonequilibrium model (DRNM), introduced elsewhere[15,19] which we shall describe only briefly. If we let $N(V,J)$ denote the level population (molecules/cm^3) and $\phi(V,J)$ the photon density (photons/cm^3) in the P-branch transition $V,J-1 \rightarrow V-1,J$ ($\phi = \rho/h\nu$ where ν is the frequency and ρ the radiation density (erg/cm^3) of the transition), the rate equations can be expressed as

$$\frac{dN(V,J)}{dt} = P(V,J) - R(V,J) + R(V+1,J-1) - D(V,J), \tag{2}$$

$$\frac{d\phi(V,J)}{dt} = R(V,J) - \phi(V,J)/\tau. \tag{3}$$

Here $P(V,J)$ is the rate of production of HCl(V,J) molecules by the pumping reaction [Eq. (1)], $R(V,J)$ is the radiative depletion rate of level V,J, $D(V,J)$ is the net depletion rate of this level by collisional energy transfer processess, (cf. Table I), and $\phi(V,J)/\tau$ is the radiation loss term.

The chemical pumping term in Eq. (2) is

$$P(V,J) = P(V) f_G^V(J), \tag{4}$$

where $P(V) = \Sigma_J P(V,J)$ is the overall pumping rate of the vibrational level V. $f_G^V(J)$ is a normalized gaussian distribution which, to a good approximation,[28] represents the nascent rotational populations in V generated by the pumping reaction. Explicitly, we set

$$f_G^V(J) = C_G^V(2J+1) \times \exp\{-B_V[J(J+1) - J_G^V(J_G^V+1)]^2/2\sigma_V^2\}, \tag{5}$$

where B_V is the rotational constant of level V, J_G^V is the most populated rotational level in V, σ_V is the width, and C_G^V is the normalization factor of the distribution. The numerical values of the constants in Eq. (5) are given in Ref. 21.

$R(V,J)$ accounts for stimulated emission, and for the small fraction (α) of spontaneous radiation along the laser axis which triggers the lasing

$$R(V,J) = g(\nu_{VJ}) B_{VJ} h \nu_{VJ}\, \Delta N(V,J) \phi(V,J) + \alpha A_{VJ} N(V,J), \tag{6}$$

where A_{VJ}, B_{VJ}, $h\nu_{VJ}$, and $\Delta N(V,J) = N(V,J-1) - N(V-1,J)[(2J-1)/(2J+1)]$ are the Einstein coefficients for spontaneous and stimulated emission, the energy, and the population inversion of the $V,J-1 \rightarrow V-1,J$ line, respectively. The line-shape function $g(\nu_{VJ})$ is taken as the Voigt profile,[27] which represents the convolution of the pressure and Doppler profiles. It is assumed that the lasing takes place at the line center and that the power extraction is homogeneous over the line profile. Variations in species compositions are explicitly included in calculating the collision broadening of the pressure profile, but the dependence on

RIGHTSLINK

vibrational and rotational quantum numbers is ignored.

The radiation loss term in Eq. (3) accounts for the useful output coupling (L_c) of photons and the dissipated losses. The photon lifetime in the cavity, τ, was set equal to $\tau^{-1} = -(C/2L)\ln[R(1-L_c)]$ in all calculations. L, the length of the laser cavity, is taken to be 60 cm.[21] $[R(1-L_c)]$ is adjusted so that there is a 10% loss of photons per round trip. It is assumed that only 20% of this loss, i.e., $L_c = 2\%$ of the total loss, appears as laser radiation. The value of α was taken to be 10^{-5}.

The relaxation term $D(V,J)$ represents the effects of rotational and various vibrational energy transfer processes on the population of level V,J. Rotational relaxation is described by the Ding-Polanyi expression for the R-T rate constant $k(J\to J';V)$, where $J > J'$

$$k(J\to J';V) = AZ(2J'+1)\exp[-C(E_J - E_{J'})], \qquad (7)$$

$$E_J = B_V J(J+1)$$

with $A = 0.05$ and $C = 0.011$ cm. Z is the collision frequency.[12] The reverse rate constant is dictated by detailed balancing. $\Delta J \geqslant 2$ transitions are excluded and it is assumed that Eq. (7) applies to all collision partners (Table I). The effects of rotational nonequilibrium on the laser performance were studied by varying the initial mixture composition $Cl_2/HI/He$.

Due to the lack of detailed information on the J dependence of vibrational relaxation rate constants of the form $k(V,J\to V',J')$ and in order to simplify the computations, we assume that these rate constants are independent of J and allow only pure V-T and V-V transitions, i.e., $J' = J$. This approximation is supported by previous studies[15,19] indicating that irregularities in the rotational distribution functions which might be caused by V-R transfer are rapidly removed by the faster R-T processes.

The set of rate equations (2) and (3) were solved simultaneously with the equations governing the time evolution of the translational temperature T and the concentration of the nonlasing species (Cl, Cl_2, HI). The total number of rate equations for the $Cl_2/HI/He$ laser system comes to 192. It should be emphasized that neither in the detailed model nor in the approximate models described below has the "gain-equal-loss" (or "on threshold"[29]) assumption for $\phi(V,J)$ [cf. Eq. (3)] been employed.

The simplest of the three laser models compared below is the one relying on the rotational equilibrium assumption, i.e., the Boltzmann equilibrium model (BEQM). Based on this assumption, one can write

$$N(V,J) = N(V) f_B^V(J), \qquad (8)$$

where $N(V) = \Sigma_J N(V,J)$ is the total population of level V and

$$f_B^V(J) = C_B^V(2J+1)\exp[-B_V J(J+1)/kT] \qquad (9)$$

is the Boltzmann rotational distribution of molecules in the V state. T is the (time-dependent) rotational-translational (or "heat bath") temperature and $C_B^V = 1/Q_R^V$ is the normalization factor; Q_R^V is the rotational partition function. Substitution of Eq. (8) into Eq. (2) and summation over J yields a well-known simplified set of vibrational rate equations.[19,27,29] This reduced set of equations, which replaces Eq. (2), involves only the sum of the pumping terms $P(V) = \Sigma_J P(V,J)$ and the average of the collisional relaxation terms (V-T and V-V) represented by $D(V) = \Sigma_J D(V,J)$. Furthermore, since at rotational equilibrium, practically, there is only one lasing line (the highest gain transition) per vibrational band, the number of nonzero photon rate equations is also small.[29] The rate equations can be further simplified by adopting the gain-equal-loss assumption leading to the replacement of Eq. (3) by an algebraic relation. However, as mentioned above, since we are interested only in the different descriptions of the rotational populations, this last assumption is not employed. (Other effects associated with the gain-equal-loss approximation in chemical lasers are discussed in Ref. 19.)

Finally we turn to the approximate rotational relaxation model (ARRM). According to this model each vib-rotational population level at any instant of time is represented as a weighted sum of the nascent-Gaussian distribution Eq. (5), the equilibrium distribution Eq. (9), and a third distribution $f_M^V(J)$,

$$N(V,J) = N_B^V f_B^V(J) + N_M^V f_M^V(J) + N_G^V f_G^V(J). \qquad (10)$$

The relative weight of each of the three distributions is given by the time-dependent superposition coefficients N_B^V, N_M^V, and N_G^V. The intermediate distribution $f_M^V(J)$ is taken to be a Boltzmann-like distribution centered around J_M^V which is an intermediate value between J_G^V [see Eq. (5)] and $J_B^V \sim (kT/2B_V)^{1/2}$, the most populated rotational level at thermal equilibrium,

$$f_M^V(J) = C_M^V(2J+1) \times \exp[-2J(J+1)/(2J_M^V+1)^2]. \qquad (11)$$

The choice of the form of Eq. (11) for $f_M^V(J)$ was based on the fact that a single parameter, J_M^V, determines both its peak and width.[21]

It should be noted that in the absence of lasing processes, which interfere with the rotational relaxation, the time evolution of the rotational distribution can often be approximated by a superposition of the nascent and the Boltzmann distributions.[26,30] The inclusion of the intermediate distribution is intended to account for two situations frequently encountered in actual cases: (1) when the nascent and Boltzmann distribution hardly overlap, (2) when the disturbances in the rotational relaxation patterns induced by the lasing and, to a lesser extent, by the vibrational relaxation processes, have a dominant effect on the overall distribution. Note however, that in the high-pressure (rotational equilibrium) limit N_G^V and N_M^V become negligible.

The practical advantage associated with this representation [Eq. (10)] is obvious. Instead of the many independent variables $N(V,J)$ in Eq. (2) the number of population variables in the present model is quite small, namely, three "subvibrational" populations N_B^V, N_M^V, and N_G^V for each vibrational level. In the absence of vibrational population transfer (via radiative transfer and relaxation processes) only R-T processes can modify the relative values of N_B^V, N_M^V, and N_G^V. The present model assumes that the relaxation from the initial, f_G^V, to the final equilibrium distribution, f_B^V, proceeds

RIGHTSLINK

TABLE II. Laser performance obtained by the three models, for various pressures (P_{tot}), at constant initial species composition ratio (Cl_2/HI/He = 4/1/4).

Model	P_{tot}	t_{Thr}[a]	t_P[b]	Energy (mJ/cm^2)						T[d]	t[e]
type	(Torr)	(μsec)	(μsec)	1→0	2→1	3→2	4→3	Total	Eff.[c]	(^{0}K)	(min)
DRNM	0.90	4.0(4→3)[f]	41.0	0.21	0.35	0.41	0.18	1.14	0.12	728	14.9
ARRM		4.0(4→3)	38.0	0.24	0.39	0.47	0.18	1.27	0.13	699	1.5
BEQM		4.0(3→2)	36.0	0.32	0.50	0.53	0.17	1.51	0.15	761	0.9
DRNM	4.50	1.8(4→3)	40.2	1.60	2.34	2.36	0.71	7.00	0.14	812	14.9
ARRM		1.8(4→3)	38.2	1.46	2.29	2.32	0.63	6.70	0.13	791	2.1
BEQM		1.8(3→2)	38.2	2.04	3.01	3.00	0.81	8.87	0.19	808	1.1
DRNM	9.00	1.4(4→3)	39.6	3.41	4.81	4.55	1.17	13.9	0.14	856	25.0
ARRM		1.4(4→3)	36.6	3.15	4.75	4.32	0.98	13.2	0.13	843	2.5
BEQM		1.2(3→2)	36.8	4.23	6.10	5.77	1.42	17.5	0.18	836	1.1
DRNM	18.0	1.0(4→3)	38.0	6.71	9.15	8.20	1.78	25.8	0.13	905	35.0
ARRM		1.0(4→3)	31.0	6.54	9.35	7.76	1.45	25.1	0.13	901	3.8
BEQM		0.9(3→2)	33.1	8.10	11.7	10.5	2.29	32.5	0.16	871	1.2
DRNM	36.0	1.0(4→3)	35.0	12.2	16.2	13.9	2.37	44.6	0.11	964	55.6
ARRM		0.9(4→3)	28.1	12.5	17.3	13.3	1.94	45.0	0.11	973	4.8
BEQM		0.8(3→2)	31.2	14.5	21.0	17.9	3.38	56.8	0.14	921	1.2
DRNM	72.0	0.8(3→2)	28.2	20.2	26.6	21.9	2.55	71.3	0.09	1022	85.2
ARRN		0.8(3→2)	25.2	21.6	29.5	21.2	2.74	74.5	0.09	1049	6.1
BEQM		0.6(3→2)	26.4	24.1	35.2	28.4	4.27	92.0	0.12	980	1.3
DRNM	144.0	0.6(3→2)	25.4	30.1	39.8	31.4	1.72	103.0	0.07	704	116.6
ARRM		0.6(3→2)	21.4	32.9	45.8	30.8	1.58	111.1	0.07	716	7.9
BEQM		0.6(3→2)	22.4	34.0	53.0	40.4	3.87	131.2	0.08	675	7.0

[a] t_{Thr} is the threshold time of the total laser pulse.

[b] t_P is the pulse length.

[c] Efficiency in terms of photons/HI molecule.

[d] All temperatures are given for time = 40.0μsec, except the 144.0-Torr run where the time = 25.0μsec.

[e] Net CPU computer time.

[f] Numbers in parenthesis indicate the vibrational band ($V \rightarrow V-1$) in which lasing starts.

via the intermediate distribution f_M^V, i.e., there is no direct population transfer from the initial to the final distribution. Rotational relaxation is thus governed by two effective deexcitation "rate constants" k_{GM}^V and k_{MB}^V (which determine the rate of passage from the initial to the intermediate and from the intermediate to the final distributions, respectively). There are no reverse rate constants since the passage to f_B^V is irreversible. The effective constants k_{GM}^V and k_{MB}^V are constructed from the state-to-state rotational relaxation constants [Eq. (7)] as follows. Using matrix notation[21] one obtains for the rotational master equation

$$\dot{\mathbf{f}} = \mathbf{K}\mathbf{f}, \qquad (12)$$

where $\mathbf{f} = \{f(J)\}$ is the vector of relative rotational populations and $\mathbf{K}$ is the rotational transition matrix where the (nondiagonal) elements are the detailed rate constants [Eq. (7)]. The formal solution of Eq. (12) is[21]

$$\mathbf{f}(t) = \exp(\mathbf{K}t)\,\mathbf{f}(0) \qquad (13)$$

and more explicitly

$$\mathbf{f}(t) = \mathbf{A}\mathbf{E}\mathbf{A}^{-1}\,\mathbf{f}(0), \qquad (14)$$

where $E_{ij} = \exp(q_i\,t)\,\delta_{ij}$, $\mathbf{A}$ is the transformation matrix of $\mathbf{K}$, and q_i are the eigenvalues. $\mathbf{f}(0)$ is the initial distribution and $\mathbf{f}(t)$ is the distribution at time t.

In the determination of k_{MB}^V the initial distribution is identified as $\mathbf{f}(0) = \mathbf{f}_M^V$. The identity $\mathbf{f}(\infty) \equiv \mathbf{f}_B^V$ is ensured by the ordinary detailed balance relations between $k(J \rightarrow J-1; V)$ and $k(J-1 \rightarrow J; V)$. Next, $\mathbf{f}(t)$ for intermediate times is represented as

$$\mathbf{f}(t) = [1 - \exp(-k_{MB}^V t)]\mathbf{f}(\infty) + \exp(-k_{MB}^V t)\mathbf{f}(0) \qquad (15)$$

which provides a good approximation to the exact relaxation pattern. The latter is given by the eigenvalue solution Eq. (13) [or equivalently by the numerical solution of Eq. (12)]. The best-fitted k_{MB}^V is then evaluated by a least-squares procedure which compares Eq. (15) with the exact solution. The evaluation of k_{GM}^V follows similar lines but with $\mathbf{f}(0) = \mathbf{f}_G^V$ and $\mathbf{f}(\infty) = \mathbf{f}_M^V$. Note, however, that in order to ensure the convergence of $\mathbf{f}(t)$ to $\mathbf{f}_M^V$, the ordinary detailed balance relation $f_B^V(J)k(J \rightarrow J'; V) = f_B^V(J')k(J' \rightarrow J; V)$ must be replaced by $f_M^V(J)k(J \rightarrow J'; V) = f_M^V(J')k(J' \rightarrow J; V)$. Further details about the ARRM concerning, for example, the effects of vibrational relaxation and stimulated emission on the overall, $N(V)$, and sub-vibrational populations, N_G^V, N_M^V, and N_B^V, are provided in Ref. 21.

III. RESULTS AND DISCUSSION

The master equations which govern the time evolution of the HCl laser system were solved in the framework of the three models:

(1) As a function of total pressure keeping the initial Cl_2/HI/He ratio constant (see Table II). The major effect of scaling up the total gas pressure is to increase the rates of the pumping reaction and vibrational relaxation. The enhancement of the total laser energy depends on the interplay between these rates.

(b) As a function of the partial inert-gas pressure while keeping the initial partial pressures of Cl_2 and HI constant

RIGHTSLINK

TABLE III. Effect of inert gas on laser performance obtained by the three models.

Model type	Initial species pressure (Torr) Cl_2	HI	He	P_{tot} (Torr)	t_{Thr} [a] (μsec)	t_p [b] (μsec)	Energy (mJ/cm ^{2}) 1→0	2→1	3→2	4→3	Total	Eff. [c]	T [d] (^{0}K)	t [e] (min)
DRNM	8.0	2.0	0	10.0	1.0(4→3) [f]	36.0	5.50	7.33	6.22	1.39	20.4	0.10	1240	26.1
ARRM					0.9(4→3)	28.1	5.07	7.26	5.98	1.20	19.5	0.10	1191	3.4
BEQM					0.8(4→3)	31.2	7.06	10.1	8.83	1.95	27.9	0.14	1201	1.2
DRNM	8.0	2.0	8.0	18.0	1.0(4→3)	38.0	6.71	9.15	8.20	1.78	25.8	0.13	905	35.0
ARRM					1.0(4→3)	31.0	6.54	9.35	7.76	1.45	25.1	0.13	901	3.8
BEQM					0.9(3→2)	33.1	8.10	11.7	10.5	2.29	32.5	0.16	871	1.2
DRNM	8.0	2.0	32.0	42.0	1.2(3→2)	40.8	8.53	12.0	11.2	2.58	34.3	0.17	590	53.7
ARRM					1.4(3→2)	37.6	8.90	12.6	10.9	1.98	34.4	0.17	599	3.2
BEQM					1.0(3→2)	39.0	9.77	14.1	12.8	2.75	39.5	0.20	571	1.1
DRNM	8.0	2.0	80.0	90.0	1.4(3→2)	44.6	9.43	14.0	13.4	3.33	40.2	0.20	475	82.2
ARRM					1.4(3→2)	41.6	10.1	14.6	12.7	2.36	39.9	0.20	490	4.2
BEQM					1.3(3→2)	43.2	10.4	15.7	14.1	2.97	43.3	0.22	464	1.2

[a] t_{Thr} is the threshold time of the total laser pulse.

[b] t_p is the pulse length.

[c] Efficiency in terms of photons/HI molecule.

[d] All temperatures are given for time = 40.0 μsec.

[e] Net CPU computer time.

[f] Numbers in parenthesis indicate the vibrational band ($V \rightarrow V-1$) in which lasing starts.

(see Table III). The major effects of increasing the inert-gas pressure are to enhance rotational relaxation and to reduce the temperature rise in the system. These effects tend to increase the laser efficiency. It is expected that this series of runs will reflect the adequacy of the three models which differ in the way the rotational relaxation is treated.

The comparison between the models is made by considering the results each gives for the following quantities:

(a) the total and vibrational output energies and efficiencies,

(b) the threshold times and duration times,

(c) the temporal behavior of the lasing output flux for the total pulse as well as for the various vibrational bands,

(d) the temporal evolution of the relative vibrational populations,

(e) the spectral distribution of the integrated output energies.

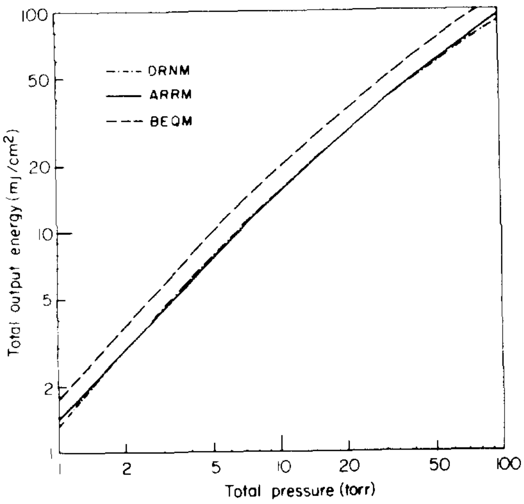

FIG. 1. The total output energy as a function of the total pressure of the lasing medium. Initial species composition ratio is kept constant, $Cl_2/HI/He = 4/1/4$.

The aim of the analysis is not only to compare the results due to the three models but also to gain a deeper insight into the physical and chemical characteristics of the lasing medium under different modes of operation.

A. Output energy and efficiency

The results obtained for the output energy, the total and the vibrational distribution, and the efficiency as calculated in the framework of the three models are given in Tables II and III and in Figs. 1–6. Laser performance as a function of the total pressure at constant initial species ratio $Cl_2/HI/He = 4/1/4$ and as a function of the partial pressure of He at constant initial partial pressures of Cl_2 (8 Torr) and HI(2 Torr) is given, respectively, in Tables II and III. The total output energy as a function of total initial pressure, and as a function of the partial pressure of He, are shown in Figs. 1 and 2. In Figs. 3 and 4 the efficiency of the system (photons per HI molecule) is given. In all cases we found that the ARRM results practically overlap the DRNM results over

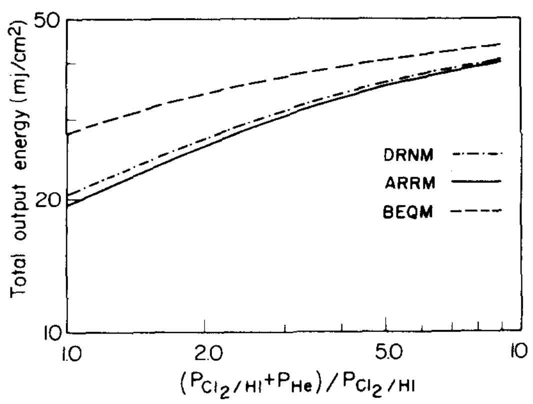

FIG. 2. The effect of enhancing the inert gas pressure (P_{He}) on the output energy, initial pressure of the reactants is kept constant, i.e., $P_{Cl_2/HI} = 8$ Torr(Cl_2) + 2 Torr(HI) = 10 Torr.

RIGHTSLINK

the entire pressure range ($\sim 1.0 - \sim 150$ Torr), whereas the BEQM results deviate significantly from the other two models.

Comparison of the results shown in Figs. 1 and 2 reveals that varying the total pressure does not affect the differences between the total output energy values obtained by the three models, whereas these differences decrease with increasing inert-gas pressure. These trends reflect the different effects of increasing the total versus the inert-gas pressure on the relative rates of stimulated emission and rotational relaxation. Increasing the He pressure enhances, almost selectively, rotational relaxation and consequently the applicability of the rotational equilibrium assumption, which is the basis of the BEQM. On the other hand by increasing both the reactant- and inert-gas pressure we increase the rate of rotational relaxation as well as the concentration of lasing molecules (hence of stimulated emission). Since the validity of the BEQM requires that R-T processes are faster than all other rate processes in the laser system, in particular stimulated emission, scaling up the concentration of all species evidently prohibits its applicability. Inspection of Figs. 1 and 3 reveals that the increase in the total output energy upon increasing the total pressure is accompanied by a decrease in the laser efficiency (except at very low pressures). On the other hand, the increase in the output energy as a function of the buffer gas pressure (Fig. 2) is a direct consquence of the increased efficiency (Fig. 4) due to the enhanced rotational relaxations and the reduced temperature, Table III. (Adding inert gas increases the heat capacity of the system. The lower temperature rise is also responsible for the increased laser efficiency predicted by the BEQM). The enhancement of laser efficiency upon increasing the R-T rates has been discussed extensively elsewhere.[14-22] The reduction in the laser efficiency displayed in Fig. 3 reflects the increasing influence of vibrational deactivation, especially due to Cl_2 and HI molecules. The low efficiency in the very low pressure regime is due to the fact that the threshold inversion is relatively large compared to the total concentration of lasing molecules [see, e.g., Ref. 18(c)]. Besides increasing the R-T rates the addition of buffer gas to the lasing mixture has a (small) effect on the efficiency due to dependence of the radiative cross section on the gas pressure. Increasing the buffer gas pressure moderates the temperature rise, thereby reducing the Doppler width. On the other hand it also increase the collisional linewidth. However the combined joint effect of these two (opposing) mechanisms on the radiative cross sections is considerably smaller than the pressure effect on the R-T rates. (Note that it is the competition between the rates of the R-T processes and stimulated emission which determines the efficiency.[14-22])

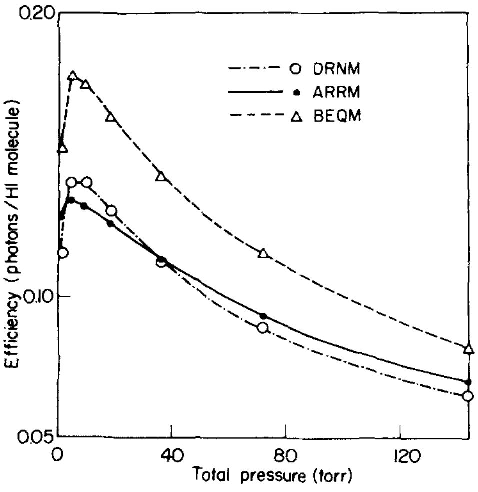

FIG. 3. The efficiency as a function of the total pressure for a constant initial species composition ratio $Cl_2/HI/He = 4/1/4$.

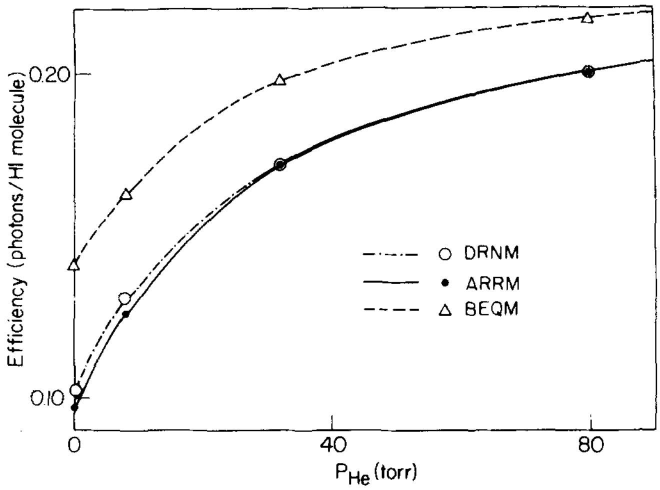

FIG. 4. The efficiency as a function of the inert-gas pressure. The reactants pressure is the same as in Fig. 2.

A more detailed comparison between the models is provided by Fig. 5 which shows the relative deviation of vibrational output energies (E^V_{ARRM}/E^V_{DRNM}) and ($E^V_{BEQM}/$

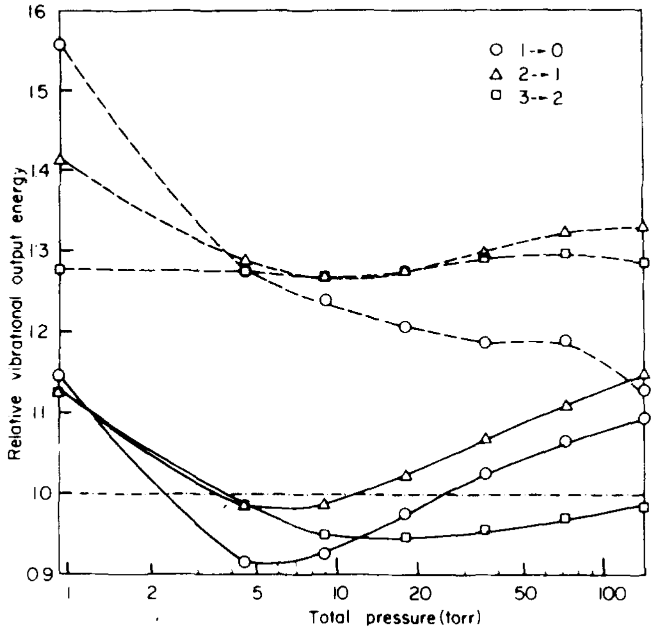

FIG. 5. Relative output energies, E_{ARRM}/E_{DRNM} (—) and E_{BEQM}/E_{DRNM} (---), of the various vibrational bands in the lasing system as a function of the total pressure. Species composition ratio is the same as in Fig. 1. The straight line(-·-), which represents the DRNM, is drawn for comparison.

RIGHTSLINK

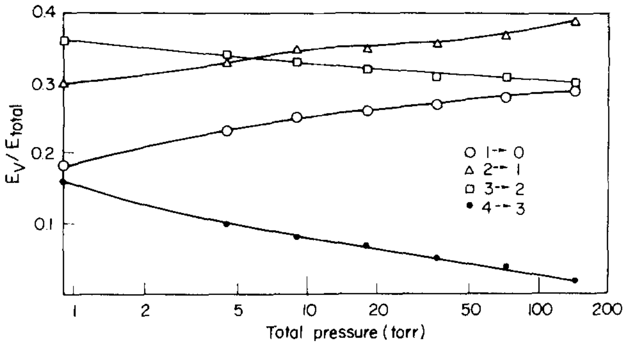

FIG. 6. Relative contributions of the various vibrational energies to the total output energy as a function of total pressure for the DRNM. Species composition ratio is the same as in Fig. 1.

$E^V_{\rm DRNM}$) as a function of the total pressure. Again it can be seen that the ARRM results are in good agreement with those of the DRNM (the largest deviation is 15% and the average deviation is less than 10%). On the other hand the BEQM results deviate significantly from those of the detailed model (sometimes as much as 50% and on the average more than 30%).

Finally, Fig. 6 (see also Table II) shows the DRNM results for the relative vibrational band intensities as a function of total pressure. As noted above, the increase in the reactant concentration involves a corresponding increase in the vibrational deactivation rates; the higher the pressure, the lower the relative intensities of the high vibrational bands (4→3) and (3→2) and the higher the relative intensities of the lower bands, (2→1) and (1→0).

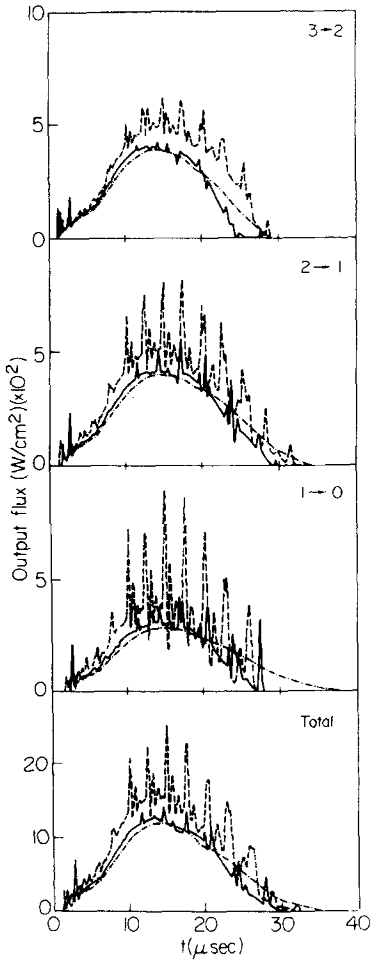

FIG. 7. The lasing output flux as a function of time for a system without buffer gas. $P_{\rm tot} = 10$ Torr, initial species composition ratio $Cl_2/HI = 4/1$. DRNM (---), ARRM (—), BEQM (---).

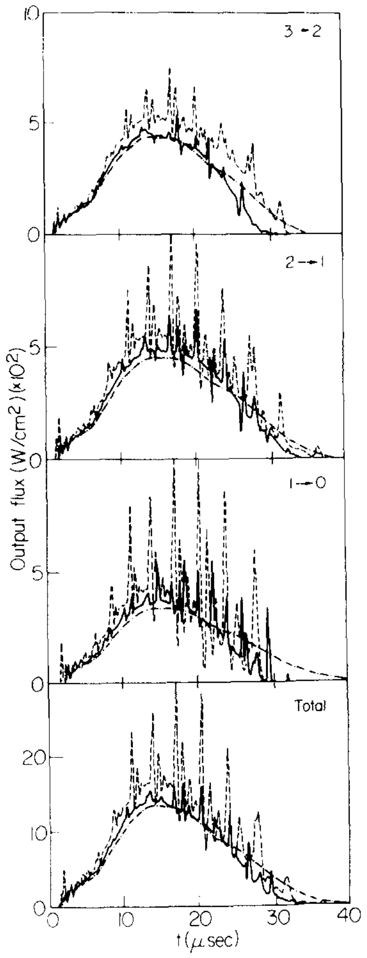

FIG. 8. The lasing output flux as a function of time for $P_{\rm tot} = 18$ Torr; initial species compostion ratio $Cl_2/HI/He = 4/1/4$. (---) DRNM, (—) ARRM, and (---) BEQM.

B. Temporal profiles of the laser pulses

The time evolution of the total output energy as well as its vibrational components yields additional detailed information on a lasing system and therefore serves as a more sensitive test of the ability of the ARRM to describe a rotational nonequilibrated lasing system. Results obtained for the three models are compared in Figs. 7 and 8 which show the time profiles of the total output pulse and of the various vibrational bands for a total pressure of 10 Torr composed of partial pressures $Cl_2/HI/He = 8/2/0$ (no inert gas), and a total pressure of 18 Torr, where the He pressure is raised to 8 Torr, respectively.

Again we note the good agreement between the ARRM and DRNM profiles. The threshold times are almost identical, the pulse shapes are similar and the peak fluxes are comparable. Deviations are only observed towards the end of the

RIGHTSLINK

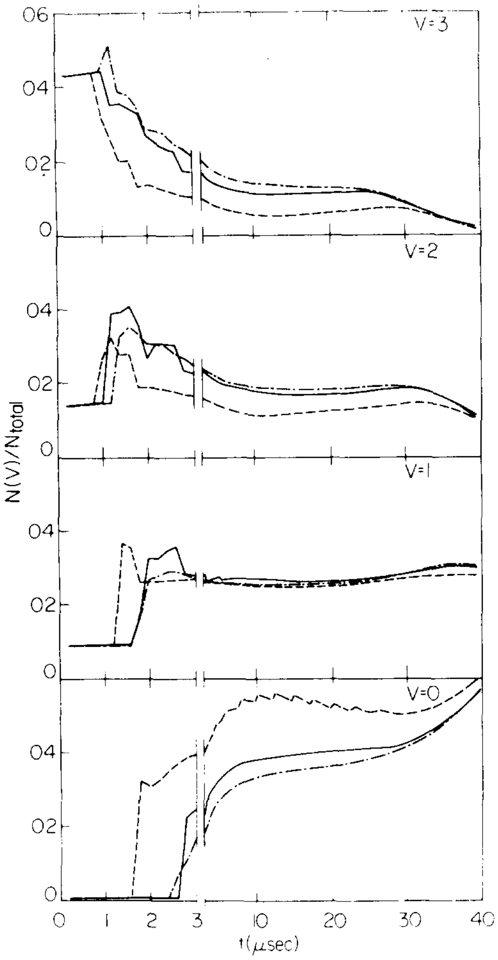

FIG. 9. Development in time of vibrational populations for a system without inert gas. P_{tot} = 10 Torr and initial species composition ratio $Cl_2/HI = 4/1$. (---) DRNM, (—) ARRM, (---) BEQM.

pulse where the ARRM pulses terminate somewhat earlier. Much more severe differences are obtained for the BEQM. These are seen not only in the sharp and strong oscillations which are typical[19] of BEQM profiles, but also in the earlier start, faster rise, and larger peak fluxes which only towards the end of the lasing become comparable to the DRNM pulses. In Sec. III C we shall see that the main contributions to the tail of the lasing are due to the higher rotational states in the band. The fact that the ARRM fails to follow the DRNM at the end of the pulse indicates that the former model does not account correctly for the populations of the higher rotational states at the final stages of the pulse. It will be shown that the ARRM somewhat overestimates the population of these states and although the differences are small they are significant enough to inhibit any additional lasing from these states.

The smooth pattern of the laser profiles as given by the DRNM reflects the simultaneous emission from the significantly populated vib-rotational states of HCl. The dented pattern of the BEQM pulse, reflects the consecutive initiation and termination of the vib-rotational pulses, namely, the J-shift phenomenon.[14-23] The fact that this structure is almost entirely eliminated by applying the ARRM is another indication of its ability to account for most of the processes during the lasing period.

By comparing Figs. 7 and 8 we can see the effect of the inert gas on the lasing system in greater detail. The effect of adding He is only minor at the early stages of the lasing (8–10 μsec) but gradually increases towards the end of the pulse. Adding the inert gas yields higher peak fluxes as well as longer lasing periods. These findings confirm again that strong rotational coupling and low temperatures enhance the lasing from partially inverted vibrational populations through high J lines.[19]

C. Level populations

1. Vibrational populations

The time evolution of the relative vibrational populations is presented in Fig. 9 for a total pressure of 10 Torr made up of partial pressures $Cl_2/HI = 8/2$ (no inert gas) and in Fig. 10 for a total pressure of 18 Torr and partial pressures $Cl_2/HI/He = 8/2/8$. As before, the fit between the ARRM and DRNM curves is good, while large deviations are seen between them and the BEQM curves. The deviations are substantial during most of the lasing period and only towards the end do they tend to disappear. The largest deviations are encountered for the $V = 0$, level which is the most sensitive to the various treatments. The reason is that the populations of all upper states ($V = 1$–4) are deter-

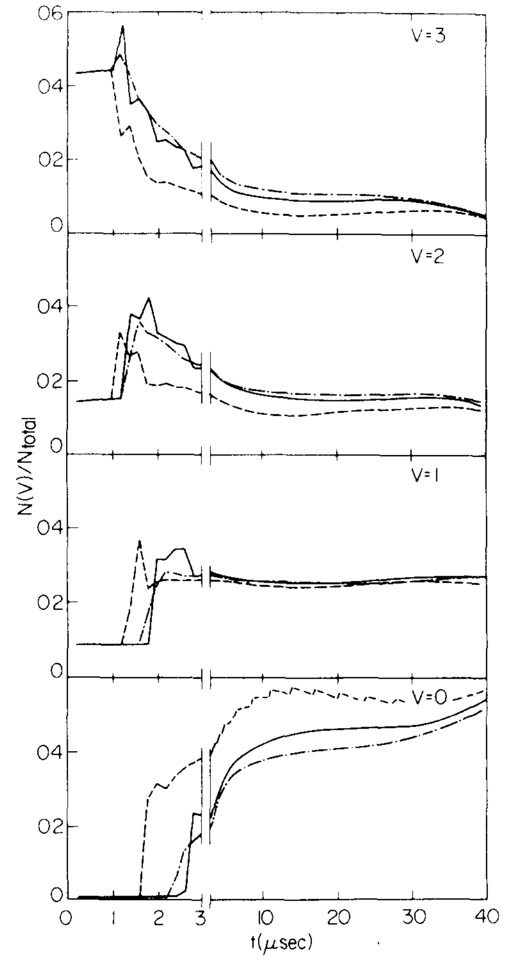

FIG. 10. The effect of inert gas on the time evolution of the vibrational populations. P_{tot} = 18 Torr and the initial species composition ratio $Cl_2/HI/He = 4/1/4$. (---) DRNM, (—) ARRM, and (---) BEQM.

RIGHTSLINK

mined by differences of fluxes, which are less sensitive to the particular treatment, while the population of $V = 0$ is determined by incoming flux alone, a magnitude which is much more model dependent.

Another set of sensitive parameters are the threshold times for the lasing which are clearly seen from the discontinuous jumps in the relative populations a few microseconds after initiation. Again the thresholds times according to the ARRM and DRNM are almost identical, whereas those due to the BEQM are always shorter. The differences result from the instantaneous concentration of most of the BEQM vibrational population in a few (low) rotational states. In the ARRM and DRNM the vibrational population is more evenly distributed among the rotational states due to the (finite-time) R-T relaxation processes. The BEQM also differs from the DRNM and ARRM in that the shortest threshold is encountered in the $3 \rightarrow 2$ transition, whereas in the other two models it is usually in the $4 \rightarrow 3$ transition (Table II). These effects have to do with the fact that $V = 3$ is the most heavily pumped vibrational state and since in the BEQM the population of this state (like any other) is instantaneously concentrated in a few rotational states, the threshold conditions for the lasing are created relatively rapidly. In the DRNM and ARRM the conditions for reaching the threshold are more involved and as a result the threshold is reached first in the $V = 4$ state.

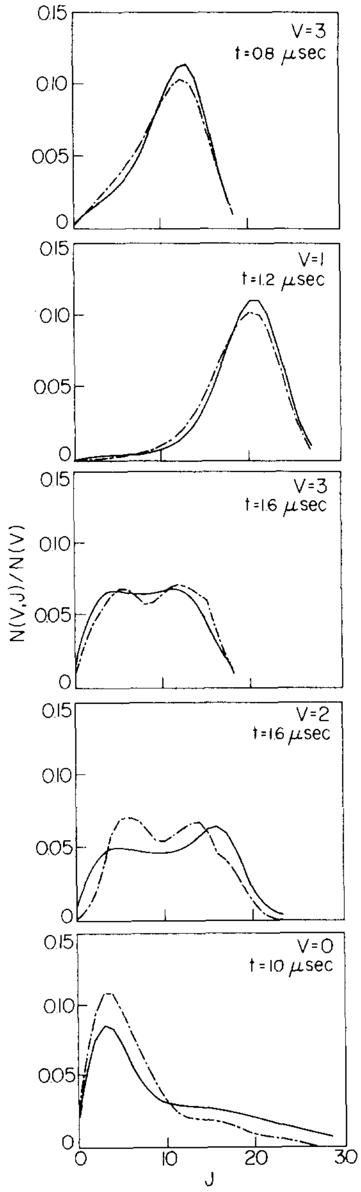

FIG. 11. Stages of rotational distribution for representative vibrational levels. The lasing system is without inert gas. The total pressure is 10 Torr and initial species composition ratio is $Cl_2/HI = 4/1$. The results for DRNM (---) and ARRM (—) are provided in terms of vibrationally normalized populations, i.e., $N(V,J)/N(V)$ for each vibrational level.

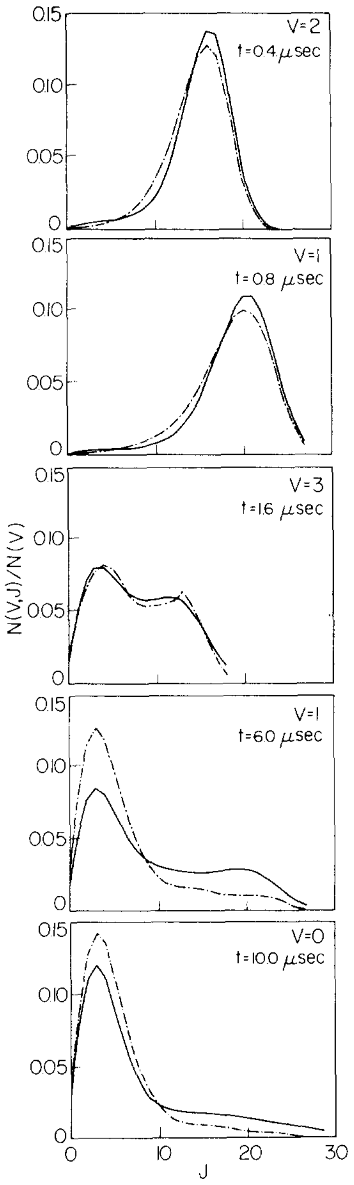

FIG. 12. The effect of inert gas on the stages of rotational distribution for representative vibrational levels. The total pressure is 18 Torr and the initial species composition ratio is $Cl_2/HI/He = 4/1/4$. (---) DRNM, (—) ARRM.

A comparison between the results plotted in Figs. 9 and 10 gives a deeper insight to the effect of the inert gas on the lasing system. Whereas in Fig. 10 (with He) the relative populations of the upper states are relatively stable, they decay in Fig. 9 due to the enhanced V-T relaxation processes which increase with temperature. It is interesting that in both cases

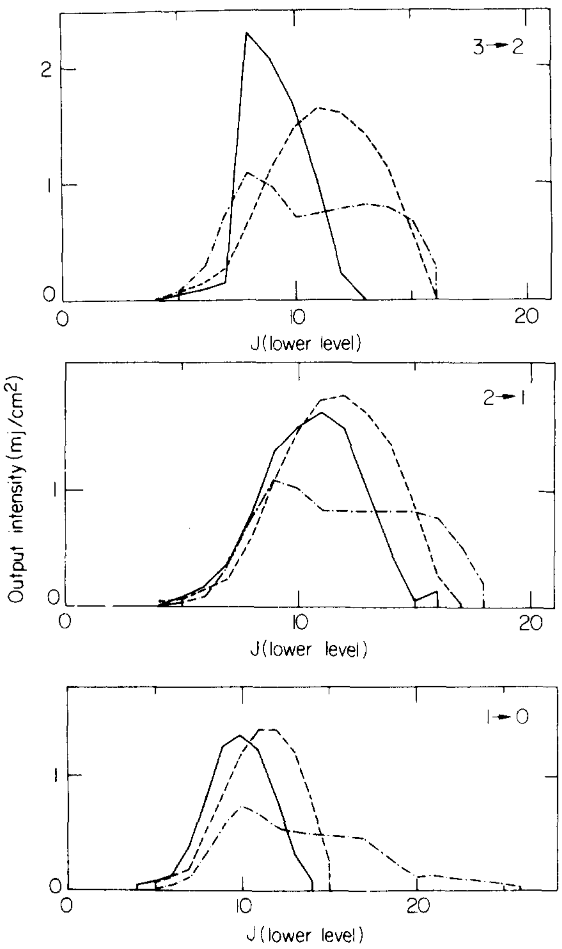

FIG. 13. The spectral distribution of the vibrational output energies. $P_{tot} = 18$ Torr; initial species composition ratio $Cl_2/HI/He = 4/1/4$. The results for each band are calculated by DRNM (---), ARRM (—), and BEQM (---).

the relative populations of $V = 1$ are almost constant throughout the lasing period.

2. Rotational populations

From Figs. 9 and 10 we observe that the time evolution of the vibrational populations is characterized by four stages. First the prethreshold region where the relative vibrational populations reflect the vibrational distribution of the nascent products of the pumping reaction. The second is the threshold region, characterized by sharp changes in these populations. Most of the laser energy is extracted in the third stage where the vibrational (partially inverted) populations are nearly time independent (reflecting a nearly steady-state operation). The fourth and final stage begins towards the end of the pulse where vibrational relaxation, which eventually carries the system to equilibrium, becomes increasingly important.

Several stages in the time evolution of the rotational distribution are illustrated in Figs. 11 and 12 where two regions are considered: (a) time before threshold is reached ($t = 0.4, 0.8, 1.6\,\mu$sec), (b) time after threshold is reached ($t = 6.0, 10.0\,\mu$sec). Figure 11 corresponds to the case without inert gas ($P_{tot} = 10$ Torr, $Cl_2/HI = 4/1$) and Fig. 12 to the case with inert gas ($P_{tot} = 18$ Torr, $Cl_2/HI/He = 4/1/4$). It can be seen that for times before threshold the distributions due to the two models are identical, but for longer times they differ in certain details. Although the bulk of the two distributions is moving toward the low rotational states at the same rate, some of the higher rotational states according to the ARRM seem to lag somewhat. In other words, the high rotational states in the ARRM are more populated than those in the DRNM (and also the BEQM) and consequently also the contribution of these states to the lasing is different.

An important fact to be noted from these results is that the main part of the lasing process takes place when the rotational populations are nearly Boltzmann. This also explains why the total output energies due to the BEQM do not differ by more than 30% from those due to the DRNM and the ARRM.

D. Spectral composition of laser pulses

The spectral distribution of the integrated output ener-

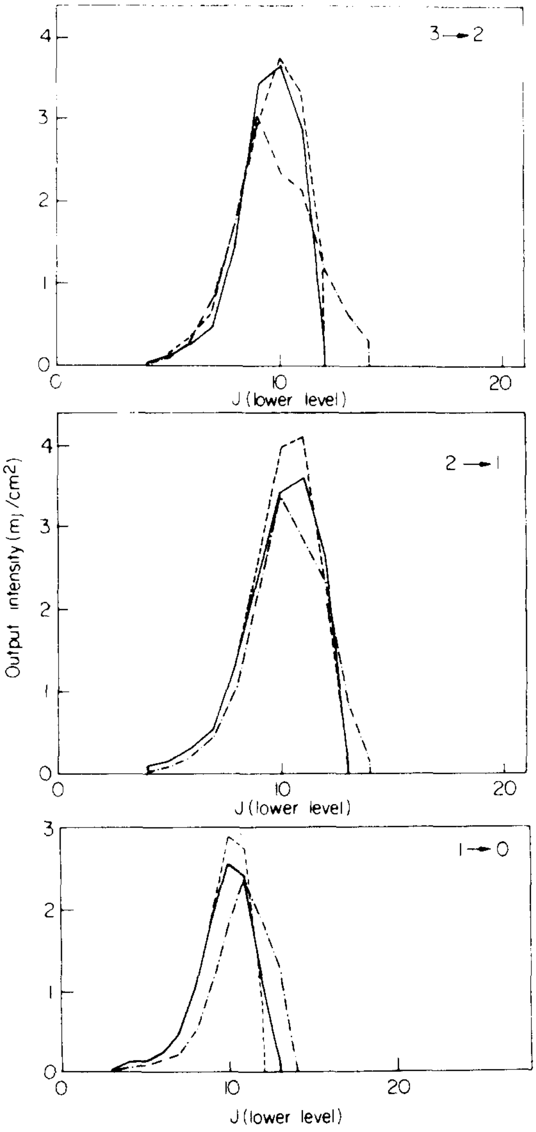

FIG. 14. The effect of excess inert gas on the spectral distribution of the vibrational output energies. $P_{tot} = 90$ Torr; initial species composition ratio $Cl_2/HI/He = 4/1/40$. (---) DRNM, (—) ARRM, (---) BEQM.

RIGHTSLINK

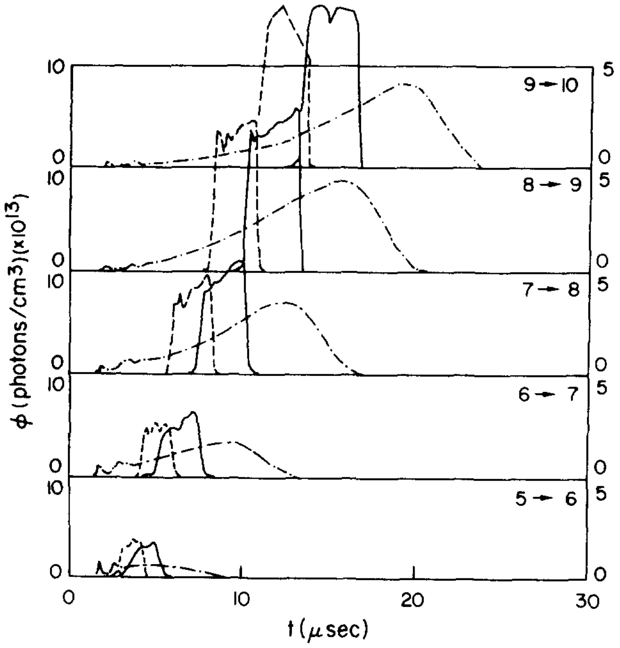

FIG. 15. A sample of photon densities for a part of the vib-rotational transitions, belonging to the 2→1 band, as a function of time. $P_{\mathrm{tot}} = 18$ Torr and the initial species composition ratio $Cl_2/HI/He = 4/1/4$. The numbers inside the figure indicate the individual $J \rightarrow J+1$ transitions. The right-hand scale refers to the DRNM results (-·-) and the left-hand scale to the ARRM (—) and BEQM (---) results.

gy provides a sensitive measure of the applicability of approximate models to obtain rotational details of chemical lasers operating under rotational nonequilibrium conditions. Figure 13 and 14 show the spectral composition of output energies for the main vibrational bands, as predicted by the three models, for slow and fast R-T relaxations, respectively. Examination of Fig. 13 reveals that the energy distribution due to DRNM in a given vibrational band is a superposition of cascading effects from the upper bands and the pumping into the vibrational levels constituting this band. For example, the spectral distribution of the 3→2 transition is divided between two peaks: the first, centered around $J = 7(\rightarrow 8)$, results from lasing in the 4 →3 band which is centered around the $J = 6$ state; the second peak, centered around the $J = 12(\rightarrow 13)$ transition, results from the initial rotational distribution in $V = 3$, which is centered around $J = 12$. At high inert-gas pressures the fast R-T rates smooth over the effects of pumping and cascading. This is true for all models and therefore the corresponding spectral distributions are similar (see Fig. 14).

E. Rotational pulses

R-T relaxation rates are strongly reflected in the temporal evolution of radiative vib-rotational transitions. A slow rotational relaxation rate is characterized by long pulses and simultaneous lasing. As the R-T rates increase, the J-shift mechanism comes into play, i.e., lasing occurs on the highest gain line, which is gradually shifted to higher J levels.

A sample of the main rotational transitions in the 2→1 vibrational band, as calculated according to the three models for conditions of intermediate R-T rate ($P_{\mathrm{tot}} = 18.0$ Torr; initial concentration ratio $Cl_2/HI/He = 4/1/4$), is presented in Fig. 15. Inspection of the pulses given by the DRNM shows that although there is rather extensive overlapping, the maxima of adjacent pulses clearly demonstrate a J-shift pattern, typical of Boltzmann conditions. This effect proves that the major part of the energy is extracted from the system which is under close to rotational equilibrium conditions.

The rotational pulses which result from the ARRM are similar to those obtained from the BEQM, namely, short, intense, and almost nonoverlapping.

IV. CONCLUDING REMARKS

The present analysis of the three kinetic models reveals that the rotational equilibrium assumption is inadequate for lasers operating under low and intermediate buffer gas pressures. In general the laser efficiencies derived on the basis of this assumption can only serve as upper bounds to the actual efficiencies. The temporal characteristics of rotational populations and pulse patterns predicted by the rotational equilibrium model are qualitatively different from those derived from the detailed solutions of the rate equations, except at very high inert-gas pressures.

The approximate model, based on a superposition representation of the vib-rotational populations, provides very good estimates for the laser energy as well as for integrated (rotationally averaged) quantities, such as vibrational populations and band intensities for a wide range of pressures. On the other hand, the details of the rotational populations and spectral distributions are not adequately reproduced by this model. However, in view of the very short computation times (see Tables II and III) required for the approximate model (compared with detailed solutions), it can be employed as an efficient tool for scanning a wide range of initial conditions. Then, if desired, the detailed (and time consuming) model can be used to obtain additional information about the laser operation.

Our major goal in this paper was to compare three approaches to the modeling of chemical lasers. This goal was motivated by the accumulation of experimental data indicating that the assumption of rotational equilibrium is not always justified. Unfortunately systematic measurements of detailed chemical laser spectra as a function of inert-gas pressures and other parameters are rarely available. Undoubtedly experiments of this kind could greatly contribute to the understanding of the complex kinetics of chemical lasers and other nonequilibrium chemical systems.

ACKNOWLEDGMENT

We thank the Israel Academy of Sciences, the Commission for Basic Research for partially supporting this work.

[1] R.F. Deutch, Appl. Phys. Lett. **10**, 234 (1967).
[2] H. Pummer and K.L. Kompa, Appl. Phys. Lett. **9**, 356 (1972).
[3] T.D. Padrick and M.A. Gusinow, Chem. Phys. Lett. **24**, 270 (1974).
[4] K.L. Kompa, *Topics in Current Chemistry* (Springer, Berlin, 1973), Vol. 37.
[5] T.D. Padrick and M.A. Gusinow, Appl. Phys. Lett. **22**, 183 (1973).

[6] M.J. Berry, Ann. Rev. Phys. Chem. **26**, 30 (1975).

[7] M.J. Molina and G.C. Pimental, IEEE J. Quantum Electron. **QE-9**, 64 (1973).

[8] (a) E. Cuellar, J.H. Padrick and G.C. Pimental, J. Chem. Phys. **61**, 422 (1974); (b) E. Cuellar and G.C. Pimental, IEEE J. Quantum Electron. **QE-11**, 688 (1975).

[9] J.J. Hintchen, Appl. Phys. Lett. **27**, 672 (1975).

[10] J.J. Hintchen and R.H. Hobbs, J. Chem. Phys. **65**, 2732 (1976).

[11] J.C. Polanyi and K.B. Woodall, J. Chem. Phys. **56**, 1563 (1972).

[12] A.M.G. Ding and J.C. Polanyi, Chem. Phys. **10**, 39 (1975).

[13] N.C. Lang, J.C. Polanyi, and J. Wanner, Chem. Phys. **24**, 219 (1977).

[14] L.H. Sentman, J. Chem. Phys. **67**, 966 (1977); **62**, 3523 (1975).

[15] A. Ben-Shaul, K.L. Kompa, and U. Schmailzl, J. Chem Phys. **65**, 1711 (1976).

[16] H.L. Chen, R.L. Taylor, J. Wilson, P. Lewis, and W. Fyfe, J. Chem. Phys. **61**, 306 (1974).

[17] J.J.T. Hough and R.L. Kerber, Appl. Opt. **14**, 2960 (1975).

[18] (a) A. Ben-Shaul, G.L. Hofacker, and K.L. Kompa, J. Chem. Phys. **59**, 4664 (1973); (b) U. Schmailzl, A. Ben-Shaul, and K.L. Kompa, IEEE J. Quantum Electron. **QE-10**, 753 (1974); (c) A. Ben-Shaul, Chem. Phys. **18**, 13 (1976); (d) A. Ben-Shaul, S. Feliks, and O. Kafri, Chem. Phys. **36**, 291 (1979).

[19] E. Keren, R.B. Gerber, and A. Ben-Shaul, Chem. Phys. **21**, 1 (1977).

[20] J.R. Creighton, IEEE J. Quantum Electron. **QE-11**, 699 (1975).

[21] M. Baer, Z.H. Top, and Z.B. Alfassi, Chem. Phys. **22**, 485 (1977).

[22] Z.B. Alfassi and M. Baer, IEEE J. Quantum Electron. **QE-15**, 240 (1979).

[23] R.J. Hall, IEEE J. Quantum Electron. **QE-12**, 453 (1976).

[24] G.K. Vasil'ev, E.F. Makarov, A.G. Ryabenko, and V.L. Tal'rose, Sov. Phys. JETP **44**, 690 (1976).

[25] (a) H.W. Chang and D.W. Sester, J. Chem. Phys. **55**, 2298 (1973); (b) J.G. Moehlmann and J.D. McDonald, J. Chem. Phys. **62**, 3061 (1975).

[26] I. Procaccia and R.D. Levine, J. Chem. Phys. **62**, 2496 (1975); **64**, 4750 (1976).

[27] G. Emanuel, in *Handbook of Chemical Lasers*, edited by R.W.F. Gross and J.F. Bott (Wiley, New York, 1976), Chap. 8.

[28] D.H. Maylotte, J.C. Polanyi, and K.B. Woodall, J. Chem. Phys. **57**, 1547 (1972).

[29] J.R. Airey, J. Chem. Phys. **52**, 156 (1970).

[30] R.D. Levine and A. Ben-Shaul, in *Chemical and Biochemical Applications of Lasers*, edited by C.B. Moore (Academic, New York, 1977), Chap. 4.

RIGHTSLINK